micro

MDPI

Article

Electrochemical-Responsive Conductive Nanofibers: A Smart Platform for DNA Storage and Controlled Release

Yang Liu [1], Yuhan Tao [1], Lili Lu [2], Zhaoxu Meng [1], He Lian [1,*] and Zhou Li [3,4,5,*]

[1] School of Medical Devices, Shenyang Pharmaceutical University, Shenyang 110016, China
[2] Wuya College of Innovation, Shenyang Pharmaceutical University, Shenyang 110016, China
[3] Vita Tech Innovation Center, Tsinghua Changgung Hospital, School of Clinical Medicine, Tsinghua Medicine, Tsinghua University, Beijing 100084, China
[4] School of Biomedical Engineering, Tsinghua Medicine, Tsinghua University, Beijing 100084, China
[5] Beijing Key Laboratory of Clinical Innovation and Translation for Active Implantable and Interventional Medical Devices, Tsinghua Changgung Hospital, Beijing 100084, China
* Correspondence: lianhe126@126.com (H.L.); li_zhou@tsinghua.edu.cn (Z.L.)

Abstract

With the exponential growth of global data volume, the physical limitations and high maintenance costs of traditional storage architectures have become increasingly prominent. DNA storage holds value in addressing these issues. However, traditional solid-phase storage media rely on chemical eluents for DNA desorption, which can easily cause the cleavage and fragmentation of nucleic acid chains, thereby interfering with the subsequent sequencing process. This study proposes an electrochemical-controlled DNA adsorption/release strategy based on a conductive composite film made of polylactic acid/polyaniline (PLA/PANI). By adopting the instant alkaline modification and in-situ wet oxidative polymerization process, the problems of interface peeling and collapse of the porous structure were avoided without compromised integrity of the PLA porous framework. Zeta potential analysis indicated that the surface charge of the film could be reversibly converted between +13.01 ± 0.10 mV and −32.53 ± 0.25 mV. Under coordinated optimization of the electrochemical stimulation and pH parameters, the composite film achieved efficient and controllable adsorption and release of DNA. This research provides a new material design concept and technical support for the construction of a green and efficient solid-phase DNA electrochemical-controlled reversible access system.

Keywords: DNA data storage; conductive composite film; polylactic acid-polyaniline; electrochemical-controlled adsorption and release; potential reversal

Check for updates

Academic Editor: Nurettin Sahiner

Received: 31 July 2026
Revised: 18 September 2026
Accepted: 29 September 2026
Published: 2 October 2026

Copyright: © 2026 by the authors. Licensee MDPI, Basel, Switzerland. This article is an open access article distributed under the terms and conditions of the Creative Commons Attribution (CC BY) license.

1. Introduction

With the rapid development of the Internet and artificial intelligence, the exponential growth of data has posed severe challenges to traditional storage architectures [1]. Currently widely used magnetic, optical, and semiconductor storage media are approaching their physical limits and are suffering from physical aging risks, necessitating periodic data migration and hardware maintenance, with associated exorbitant operational costs [1–3]. In contrast, DNA, as a natural genetic information carrier, relies on its stable phosphodiester backbone and the specific linear arrangement of nucleobases (A, T, C, G) to achieve ultrahigh data storage density [3–5], high fidelity, and extremely low maintenance energy consumption. Therefore, it has emerged as a highly promising material for solid-state storage media [6–9].

A complete DNA data storage system encompasses not only high-throughput data writing (synthesis) and decoding (sequencing), but also highly relies on the carrier for efficient management and non-destructive access to massive DNA pools [8]. The traditional liquid-phase storage is susceptible to DNA hydrolysis and backbone cleavage, leading to permanent data loss [7,10]. To address this challenge, researchers have turned to solid-phase matrices and utilized interfacial electrostatic interactions to achieve reversible DNA immobilization [4,6,11,12]. For example, porous cellulose paper [6], aminated polyethersulfone membranes [11], and porous photonic microspheres [4] have successfully achieved highly efficient DNA retrieval. However, the desorption process from conventional solid-phase media is highly dependent on the regulation of the macroscopic environment and requires frequent replacement of high-salt eluents. This chemical elution procedure is not only cumbersome but also prone to induce loss of nucleic acid fragments, and the residual chemical reagents can also contaminate the downstream microfluidic chip integration and the preparation of sequencing libraries [1,2,11]. Therefore, the construction of an electrochemical-controlled DNA adsorption/release medium under mild conditions is a vital driving force for the development of DNA storage technology.

Electrospinning technology, as an efficient nanofiber fabrication method, provides unique advantages for constructing 3D network solid-phase carriers with high porosity and high specific surface area [13–16]. Among various polymer matrices, poly (lactic acid) (PLA), an environmentally friendly polymer [17,18], possesses excellent thermal processability, mechanical flexibility, and biocompatibility [18–22], thus becoming an ideal backbone material for constructing flexible solid-phase storage films [23–26]. However, the unmodified PLA films suffer from high hydrophobicity [27,28] and intrinsic electrical insulation, which severely impedes their responsiveness to electrochemical drive [27,29]. Therefore, introducing a highly conductive and electrochemically reversible functional layer onto the porous backbone surface of PLA is crucial for achieving electronically controlled DNA access.

Conjugated conductive polymer polyaniline (PANI) has emerged as a prime choice for the electroactive modification of insulating frameworks due to its unique intrinsic conductivity and reversible protonation/deprotonation switching mechanism [30–35]. Previously, researchers attempted to introduce PANI into PLA substrates by direct blending [28,36] or through in situ chemical oxidative polymerization [27,36], in order to enhance the conductivity and wettability of the material. However, the physical blending method tends to encapsulate conductive particles within the polymer matrix. Moreover, the traditional in-situ coating suffers from weak interfacial bonding and is prone to delamination, and intense drying process may damage the porous framework [27,37]. Furthermore, PLA/PANI composite materials are predominantly applied in environmental remediation and tissue engineering [23,27,37], and their potential in digital DNA storage has not been fully exploited.

To address these challenges, this study has developed a new type of conductive composite film (PLA/PANI) for electrochemical-controlled DNA storage. Using porous electrospun PLA nanofibrous membranes as the substrate, hydrophilic functional groups were introduced via localized surface hydrolysis through brief alkaline modification, followed by the directly in situ wet polymerization of PANI without an intermediate drying step. This strategy successfully established highly wettable electronic transport pathways while maintaining the flexible porous structure of PLA. By taking advantage of the reverse protonation characteristics of PANI under different voltages and pH conditions, the efficient and reversible electrochemical-controlled adsorption and release of target DNA molecules have been achieved. This study systematically explores the preparation process, microscopic morphology, and electrochemical-controlled DNA capture mechanism of the

PLA/PANI composite film, aiming to provide a new strategy for the development of smart DNA data storage and random retrieval media.

2. Materials and Methods

2.1. Materials

Polylactic acid (PLA, 110 kDa) was purchased from Macklin (Shanghai, China). Aniline (99.5%) and ammonium persulfate (APS, 98.0%) were obtained from Aladdin (Shanghai, China). Hexafluoroisopropanol (HFIP, 99.5%) was purchased from Leyan (Shanghai, China). The pUC57 plasmid was custom synthesized by GenScript. 2× TransStart Fast PCR SuperMix (Fly Mix) and nuclease-free water were obtained from TransGen Biotech (Beijing, China). PCR primers (31-PCR, 51-PCR and UL2) were synthesized by Sangon Biotech (Shanghai, China). High-resolution agarose, SafeRed nucleic acid gel staining agent (10,000×), 50× TAE buffer and DEPC-treated water were provided by Feimo Biotechnology (Beijing, China). 6× DNA loading buffer was purchased from Solarbio (Beijing, China). The plasmid purification buffers (including binding buffer NTI, washing buffer NT3 and elution buffer NE) were purchased from MACHEREY-NAGEL (Düren, North Rhine-Westphalia, Germany). Analytical pure phosphoric acid (H_3PO_4) was purchased from Tianjin Kemao (Tianjin, China). Acetic acid, hydrochloric acid, boric acid and sodium hydroxide (all analytical pure) were provided by Rionlon Bohua (Tianjin, China).

2.2. Experimental Section

2.2.1. Preparation of PLA/PANI Conductive Composite Films

In this study, PANI was introduced onto the surface of flexible PLA nanofiber membranes to fabricate conductive composite films. First, for the preparation of PLA nanofiber membranes, 0.14 g of PLA was fully dissolved in 1 mL of 1,1,1,3,3,3-hexafluoro-2-propanol (HFIP) under magnetic stirring at 25 °C for 4 h to prepare a 14% (*w*/*v*) electrospinning solution. Subsequently, the solution was filled into a syringe equipped with a flat-head needle and mounted onto the HZ-10 electrospinning machine (HZ Electrospinning, Qingdao, China). The electrospinning parameters were set as follows: an applied working voltage of 14 kV, a tip-to-collector distance of 10 cm, and a syringe pump flow rate of 1.0 mL/h. The collected pure PLA nanofiber membranes were dried at room temperature for 24 h to completely remove residual solvents.

Subsequently, the dried pure PLA nanofiber films (2 cm × 2 cm) underwent interfacial alkaline modification. The films were immersed in the alkaline modification solution (prepared by mixing a 0.05 M NaOH solution with anhydrous ethanol in a ratio of 1:1 (*v*/*v*)) for 5 s, ensuring that only surface hydrolysis occurred without compromising the integrity of the fibers. This process triggers local hydrolysis of surface ester bonds, thereby introducing hydrophilic functional groups, such as carboxyl (–COOH) groups in situ.

The modified films were directly placed into the polymerization system. The polymerization solution was prepared by dissolving 500 µL of aniline monomer in 40 mL of 0.5 M hydrochloric acid (HCl) solution and continuously stirring until complete protonation. The oxidant solution was prepared by completely dissolving 0.9 g of ammonium persulfate (APS) crystals in 10 mL of 0.5 M HCl. The pre-wetted modified PLA films were initially immersed in the aniline–HCl solution for 10 min to promote the surface adsorption of aniline molecules onto the porous fibers. Subsequently, 10 mL of the oxidant solution was introduced into the reaction system. The reaction container was then transferred to a horizontal shaker (100 rpm, 20 °C) to undergo in situ chemical polymerization for 3 h. During this period, the films gradually changed from milky white to dark emerald green due to the construction of the conjugated conductive network. After the reaction, the films were washed sequentially with 0.5 M HCl, ultrapure water, and anhydrous ethanol to remove

residual monomers and by-products. Finally, the films were dried at room temperature for 24 h to obtain the PLA/PANI conductive composite films.

2.2.2. Characterization and Measurements

The surface microstructure morphology of the pure PLA nanofiber films and the PLA/PANI conductive composite films was observed via scanning electron microscopy (SEM, JCM-7000 NeoScope, JEOL, Tokyo, Japan). To measure the average diameter of the nanofibers, 60 random diameter measurements were recorded in SEM images (Figure 1b,d) by using Fiji software (ImageJ 1.54p, macOS ARM64 version). The characteristic chemical bonds and molecular structures of the samples were verified by Fourier transform infrared spectroscopy (FTIR, Nicolet iS20, Thermo Scientific, Waltham, MA, USA) in attenuated total reflection (ATR) mode within a scanning range of 4000–400 cm^{-1}. The surface electron transport efficiency of the films was evaluated using a four-probe tester (ST2253A, Suzhou Jingge Electronic Co., Ltd., Suzhou, China) to determine the volume resistivity of the composite films. Four metal probes were arranged in a straight line at equal intervals and pressed vertically onto the film surface. The outer two probes supplied a known constant current, while the inner two probes measured the potential difference with a high-impedance voltmeter. The macroscopic interfacial wetting properties of the films before and after modification were quantitatively assessed using a contact angle goniometer (JY-82C, Chengde Dingsheng, Chengde, China) by recording the static contact angles of deionized water on the film surfaces via the sessile drop method.

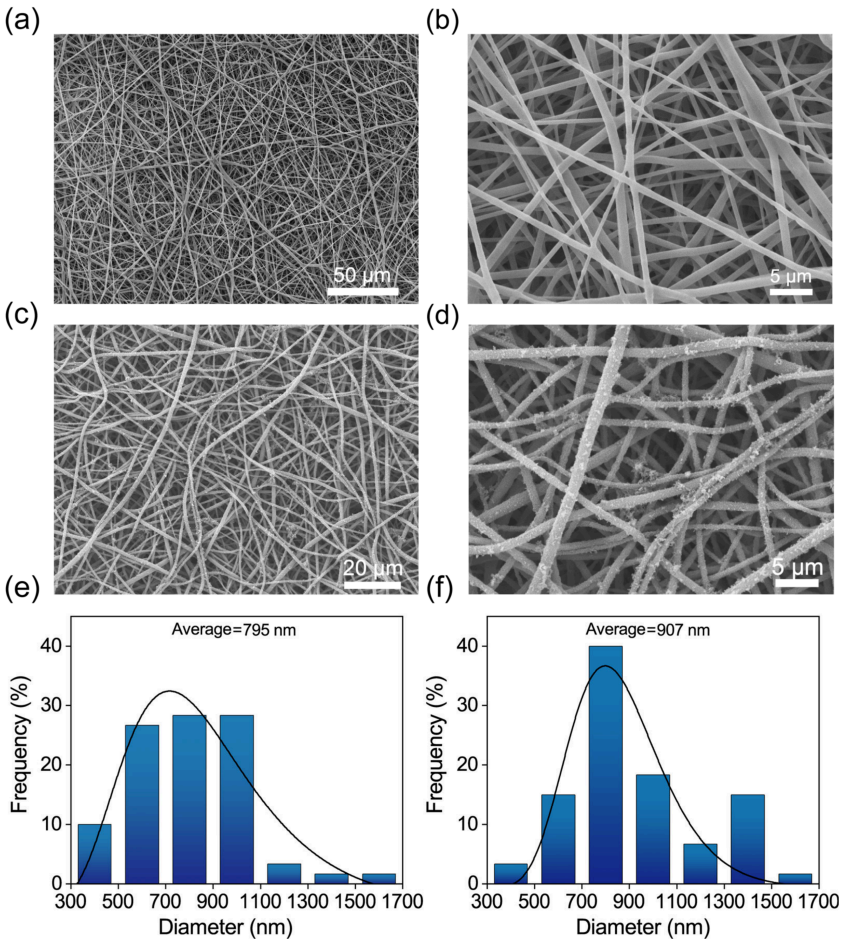


Figure 1. SEM images of the films and the corresponding fiber diameter distribution profiles: (**a**) pristine PLA (500×); (**b**) pristine PLA (3000×); (**c**) PLA/PANI (1000×); and (**d**) PLA/PANI (3000×); (**e**) histogram of PLA fiber diameter; (**f**) histogram of PLA/PANI fiber diameter.

To evaluate the electrochemical response and surface charge regulation of the composite membrane under working conditions, the surface zeta potential inversion behavior was dynamically traced using a solid surface zeta potential analyzer (Surpass 3, Anton Paar GmbH, Graz, Austria) across a pH range of 3.0 to 10.0. Meanwhile, a standard three-electrode electrochemical system was constructed: the prepared conductive composite film was used as the working electrode, the platinum plate electrode as the counter electrode, and the saturated calomel electrode (SCE) as the reference electrode. The cyclic voltammetry (CV) characteristics of the interface were evaluated using an electrochemical workstation (CHI660E, CH Instruments, Shanghai, China) in an acidic Britton–Robinson (BR) buffer solution (pH 3.0) to assess its capacitive properties. In addition, tensile fracture tests of the film before and after modification were conducted using a universal testing machine (UTM2102, Shenzhen Sansi Zongheng, Shenzhen, China) to quantitatively evaluate the mechanical properties, including tensile modulus and fracture elongation rate.

2.2.3. PCR Amplification, Purification, and Quantification of the Target DNA Fragment

The 1300 bp target DNA fragments were prepared via polymerase chain reaction (PCR) amplification using a pUC57 plasmid as the reaction template. The standard 50 μL PCR reaction system included: 1 μL of plasmid template, 25 μL of 2× TransStart Fast PCR SuperMix, 2.5 μL of the upstream 5′ primer (5 μM), 2.5 μL of the downstream 3′ primer (5 μM), and finally 19 μL of nuclease-free water. After mixing and centrifugation, the PCR reaction tubes were placed in the Gene Explorer PCR instrument (BIOER, Hangzhou, China) for amplification. The program was set as follows: 98.0 °C for pre-denaturation for 2 min; then 35 cycles of amplification (98.0 °C denaturation for 15 s, 46.7 °C annealing for 10 s, 72.0 °C extension for 30 s); and finally 72.0 °C for extension for 2 min.

Subsequently, the amplified products were separated using 2% (*w*/*v*) high-resolution agarose gel electrophoresis. The gel matrix was prepared by dissolving 3.2 g of agarose powder in 160 mL of 1× TAE buffer, which was obtained by diluting the 50× TAE stock with deionized water. Then the suspension was completely melted via microwave heating and supplemented with SafeRed nucleic acid gel stain. The collected PCR products were mixed with 6× DNA loading buffer and loaded into the gel wells, with a D2000 DNA Marker serving as the molecular weight standard. Electrophoresis was then carried out in a horizontal electrophoresis tank connected to a DYY-6D power supply (Beijing Liuyi, Beijing, China) at a constant voltage of 70 V for 1 h.

After electrophoresis, the target 1300 bp DNA bands were visualized and located under ultraviolet (UV) light using a Tanon 1600 gel imaging system (Tanon, Shanghai, China). The corresponding target gel blocks were excised and weighed, followed by extraction and recovery using a NucleoSpin plasmid purification kit (MACHEREY-NAGEL, Düren, North Rhine-Westphalia, Germany). The excised gel blocks were mixed with NTI binding buffer at a weight-to-volume ratio of 1:2 (*w*/*v*) and incubated in a constant-temperature metal bath (50 °C, 300 rpm) for 50 min until complete dissolution. The dissolved solution was then transferred to a silica membrane spin column and centrifuged at 11,000× *g* for 30 s to discard the waste liquid. Subsequently, the column was washed with 700 μL of NT3 washing buffer and centrifuged once again to remove residual ethanol. Finally, a new collection tube was replaced, and 18 μL elution buffer was added to the silica membrane for elution. After standing for 1 min, the purified DNA solution was collected via centrifugation at 11,000× *g* for 1 min. Eventually, the concentration and purity of the harvested DNA were determined using a NanoDrop One^{c} spectrophotometer (Thermo Scientific, Waltham, MA, USA).

2.2.4. Electrochemical-Controlled DNA Adsorption/Release Behavior and Optimization

To evaluate the structural integrity of the target DNA molecules (1300 bp) during the reversible adsorption/release process in a solid-phase medium, this study first verified their stability within the simulated working window. In the acid–base tolerance experiment, DNA samples at a constant initial concentration were incubated in BR buffer solutions (pH 3.5 and 10.0) for 3 h, with 3 μL of the reaction mixture collected every 30 min. Subsequently, a voltage safety testing system was constructed: a filter paper strip pre-wetted with BR buffer solution served as the working electrode, with its top end secured by an iron clip and its bottom end vertically immersed in the DNA solution; a platinum sheet electrode was used as the counter electrode. A constant positive potential of +0.7 V was continuously applied using a DC regulated power supply for 3 h (with samples collected every 30 min). All harvested samples were analyzed by agarose gel electrophoresis to quantitatively evaluate the intensity of specific characteristic bands, thereby determining the safe voltage range and pH stability window.

Having defined the safety window, PLA/PANI conductive composite films (6 mm × 6 mm) were used to investigate the electrochemically controlled adsorption and desorption processes of DNA. Electrochemical-controlled adsorption stage: the composite film was used as the working electrode and a platinum sheet as the counter electrode. Both electrodes were immersed in 120 μL of BR buffer solution (pH 3.5) containing target DNA. A constant positive voltage of +0.7 V was applied for 2 h to drive DNA migration. The control group without external electrochemical stimulation (0 V) was tested under the same conditions. After the electric field supply, the adsorbed film was briefly rinsed with ultrapure water and then transferred to 120 μL of pH 10.0 BR buffer solution. Electrochemical-controlled desorption stage: to induce desorption, a negative potential of −0.7 V was applied for 4 h (the film as the cathode, platinum sheet as the anode). To quantitatively assess the effect of the external electrochemical stimulation on the acceleration efficiency of DNA migration, 3 μL of solution was collected every 1 h from both the residual adsorption mixture and the eluate for gel electrophoresis analysis.

To meet the requirements of rapid response and extended cyclic stability for practical applications, the processing parameters during both the DNA adsorption and release stages were optimized:

(1) Voltage optimization during the adsorption stage: in a buffer solution at pH 3.5, constant positive potentials (+0.6, +0.7, and +0.8 V) were individually applied to the system for 3 h. Samples were collected every 1 h for electrophoresis analysis.

(2) Synergistic optimization of pH and voltage during the release stage: first, under a constant reverse potential of −0.7 V, the pH of the elution buffer was adjusted to 8.0, 9.0, and 10.0, respectively, and the DNA release efficiency was evaluated regularly within 3 h. Subsequently, in the optimized alkaline environment (pH 10.0), the reverse potential (−0.6, −0.7, and −0.8 V) was used to conduct electrochemically induced desorption for 3 h, respectively. The optimal operating conditions for DNA adsorption and release were finally established.

3. Results and Discussion

3.1. Fabrication and Characterization of PLA/PANI Conductive Composite Films

To develop a low-cost, high-surface-area storage medium, this study proposes a composite film fabrication strategy based on the in-situ growth of a reversible charge layer on an electrospun scaffold. The system involved three consecutive steps in its fabrication: firstly, PLA was electrospun into a highly porous nanofibrous substrate; secondly, brief alkaline treatment induced surface ester hydrolysis to expose carboxyl (–COOH) active sites; next, the modified film was placed in an acidic aniline monomer solution, and the in-situ chemical polymerization reaction was initiated upon adding an oxidant. Eventually, a

continuous conductive PANI functional layer was constructed on the surface of the flexible insulating PLA framework.

SEM images illustrate the morphological evolution of the composite film. The untreated PLA nanofibers (Figure 1a,b) exhibit a smooth, bead-free 3D interconnected network. This porous topology provides an optimal substrate for the immobilization of the electroactive layer. After in-situ PANI polymerization, the granular PANI nanoclusters densely coat on the nanofiber framework (Figure 1c,d). Consistent with this morphological transformation, quantitative statistical analysis (Figure 1e,f) reveals that the average fiber diameter increases from 795 nm (pristine PLA) to 907 nm after PANI coating. The black solid line represents the log-normal fit of the fiber diameter distribution. This confirms the successful construction of a continuous charge-conduction pathway while maintaining the high specific surface area of the substrate. The FTIR spectra (Figure 2a) elucidate the chemical composition and interfacial bonding mechanism of the composite film. Both alkaline-treated PLA and PLA/PANI films completely retained the characteristic peaks of the PLA matrix, including C=O stretching (1751 cm^{-1}) and C–O–C asymmetric and symmetric stretching (1181 and 1084 cm^{-1}) [27,28]. For the alkaline-treated film, the emergence of a carboxylate ($–COO^-$) peak at 1594 cm^{-1} confirms surface ester cleavage and the introduction of hydrophilic groups. For the PLA/PANI film, other characteristic peaks of polyaniline were also observed: the C=C/C=N stretching vibration of the quinone ring was at 1579 cm^{-1} and the C=C stretching vibration of the benzene ring was at 1495 cm^{-1} [27,28]. These spectral features confirm the successful coating of an electroactive PANI layer on the PLA fiber surfaces.

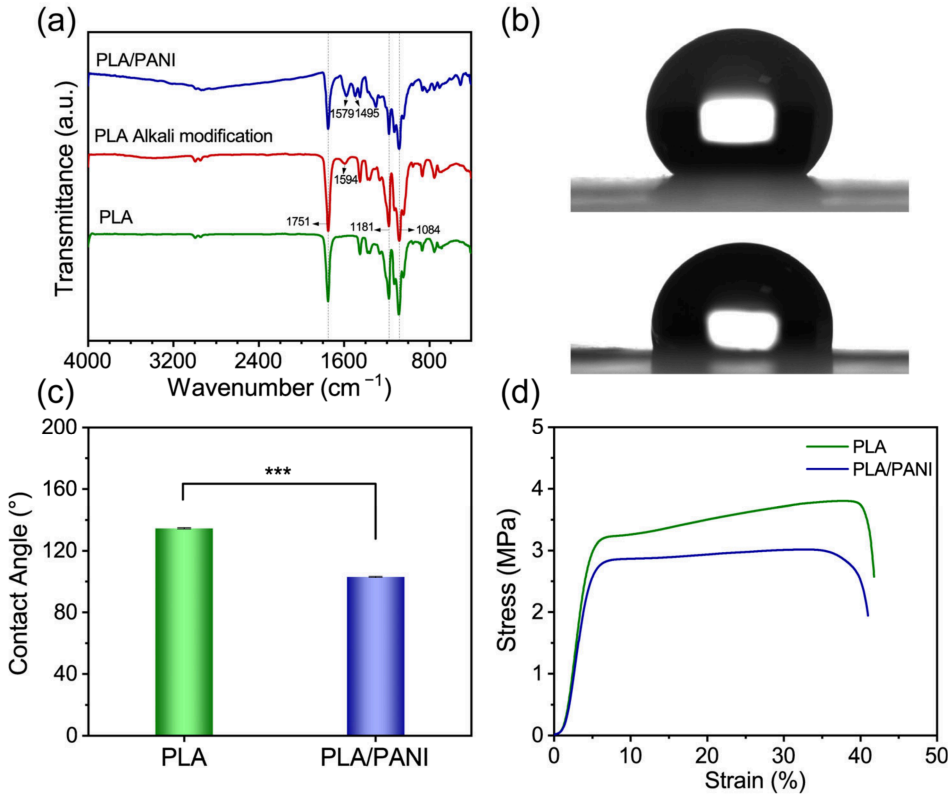


Figure 2. Characterization of the films. (**a**) FTIR spectra of pristine PLA, alkali-treated PLA, and PLA/PANI composite film; (**b**) water contact angle images of the films; (**c**) corresponding statistical histogram of contact angles (n = 3, Mean ± SD, *** $p < 0.001$); (**d**) stress–strain curves of the films before and after modification.

The introduction of these surface functional groups directly regulated the interfacial physicochemical properties of the composite films. The contact angle measurements (Figure 2b) reveal that the pristine PLA film exhibits strong hydrophobicity with a high water contact angle (WCA) of 134.50 ± 0.42°, severely preventing water penetration. After a brief alkaline modification and in-situ PANI polymerization, the WCA of the PLA/PANI composite film decreases significantly to 103.01 ± 0.42°. This improvement in wetting properties confirms that the modification effectively enhances hydrophilicity, facilitating the penetration and diffusion of aqueous DNA solutions into the porous network. Furthermore, the representative tensile stress–strain curves (Figure 2d) obtained via a universal testing machine demonstrated that the in situ wet processing strategy did not cause any structural damage to the original physical flexibility of the electrospun mesh. This mechanical robustness fulfills the physical integrity required to withstand repeated deformation during adsorption/desorption cycles.

3.2. Electrochemical Activity of PLA/PANI Composite Films and Reversible Surface Charge Regulation Mechanism

The electrochemical conductivity of the film within the mild voltage window is the key metric determining its applicability for efficient DNA storage. The four-probe resistivity test (Figure 3a) reveals that the composite film polymerized in 0.5 M HCl achieves a markedly lower volume resistivity than the sample polymerized in 1.0 M HCl. Under strongly acidic conditions (1 M HCl), the rapid reaction kinetics cause PANI to undergo uncontrolled "secondary growth" on the nanofiber surface, resulting in the deposition of rough and irregular polymer aggregates that disrupt the continuity of the PANI network on the PLA fiber surface [38]. In contrast, the milder acidic environment (0.5 M HCl) effectively slows the reaction and prevents secondary growth, allowing aniline to polymerize into a more coherent PANI conductive network across the porous fibers, thereby enhancing the electron transport capability.

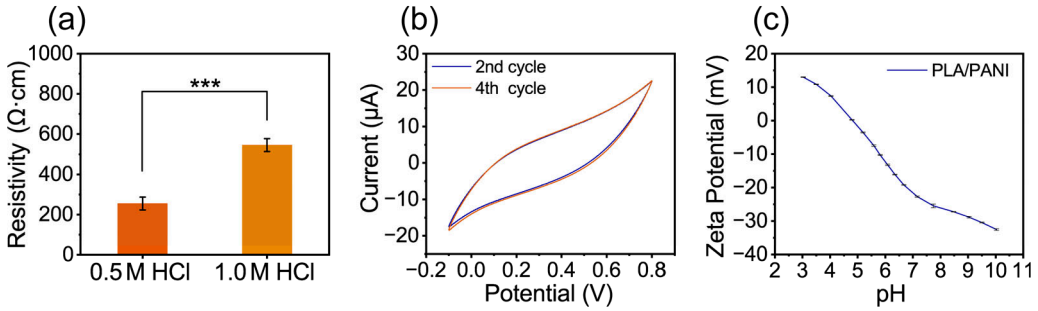


Figure 3. Electrochemical characterization. (**a**) Volume resistivity of PLA/PANI composite films prepared with 0.5 M and 1 M HCl (n = 3, Mean ± SD, *** $p < 0.001$); (**b**) CV curve of the PLA/PANI composite film; (**c**) Zeta potential curve of the PLA/PANI composite film.

The electrochemical activity of the film was evaluated by cyclic voltammetry (CV) in a standard three-electrode cell. The film was subjected to four cycles of scanning. To eliminate the activation effect of the first cycle, the second cycle was selected as the representative of the initial state and the fourth cycle as the stable state (each cycle included two scans in both positive and negative directions). As shown in the figure (Figure 3b), as the number of scanning cycles increased from two to four, the peak current slightly decreased and stabilized. The curve exhibited a full contour and excellent symmetry, demonstrating the characteristics of a quasi-capacitive redox reaction. This superior activity enables the film to accumulate dense surface charges under positive potentials in acidic media, facilitating strong electrostatic interaction with the negatively charged DNA phosphate backbone.

To observe the reversible surface charge inversion performance of the PLA/PANI composite film in response to the changes in environmental pH, the Zeta potential was dynamically measured using a solid-surface Zeta potential analyzer (Figure 3c). The results showed that under acidic electrolyte (pH 3) conditions, the film surface exhibited a significant positive charge characteristic, with a Zeta potential of +13.01 ± 0.10 mV. Upon switching to pH 10, the Zeta potential sharply reversed to −32.53 ± 0.25 mV. This significant Zeta potential reversal phenomenon proves that the composite film has a highly reversible interface charge conversion ability. Further mechanism analysis indicates that this reversible switching of the interface charge state is the core mechanism driving the efficient adsorption and release of DNA: under acidic and positive bias conditions, the amine/imine functional groups on the PANI molecular chains undergo sufficient protonation (transforming into $=NH^{+}-$ and $-NH_2^{+}-$), forming a green salt-like (ES) with high positive charge density, which can generate strong electrostatic attraction with the negatively charged phosphate groups ($-PO_4^{-}$) on the DNA backbone, thereby achieving efficient capture of DNA; when the environment switches to alkaline and reverse bias conditions, PANI undergoes deprotonation, causing the overall potential of the film to reverse to a negative value, and then generating a strong electrostatic repulsion with the $-PO_4^{-}$ groups of DNA, driving the efficient desorption of DNA.

3.3. Electrochemical-Guided DNA Adsorption/Release and Parameter Optimization

Firstly, the structural stability of DNA in acidic and alkaline microenvironments and under an applied electrochemical stimulation was evaluated. The acid–base tolerance test (Figure 4a) showed that DNA incubated for 3 h at 37 °C in BR buffers (pH 3.5 and 10.0) had the same gray intensity of the bands as the untreated original control group (lanes 1 and 8), and no low-molecular-weight diffuse tails were observed, confirming that the strong acid/strong base microenvironment did not cause the hydrolysis and breakage of DNA phosphodiester bonds. The voltage safety assessment (Figure 4b) further verified the structural integrity under electrochemical stimulation. After continuous application of +0.7 V stimulation for 3 h, no decrease in gray level or shift in electrophoretic mobility was observed for the DNA characteristic bands. The band contours were identical to the control group that did not receive any voltage (lane 1). These findings demonstrate that DNA remains intact within the pH range of 3.5 to 10.0 and the voltage range of +0.7 V, establishing a secure working window for subsequent adsorption and release.



Figure 4. Gel electrophoresis analysis of DNA stability. (**a**) Stability of DNA in different BR buffers for 3 h (pH 3.5 and 10.0) (lanes 1/8: controls; lanes 2–7 and 9–14: pH 3.5 and 10.0 incubations at 30-min intervals). (**b**) Stability of DNA under +0.7 V electrochemical stimulation for 3 h (lane 1: control; lanes 2–7: 0.5 to 3 h).

Subsequently, a closed-loop evaluation of electrochemical-controlled DNA adsorption and desorption was then performed using the PLA/PANI conductive composite film (Figure 5a). Gel electrophoresis analysis revealed that during the capture stage, compared

with the original DNA stock solution (lane 1), the intensity of the residual DNA bands in the supernatant of the electrochemical-applied group (+0.7 V, pH 3.5; lanes 2–3) decreased sharply, significantly lower than that of the passive adsorption control group (0 V, pH 3.5; lanes 4–5), indicating that DNA was efficiently captured onto the film surface under the electrochemical drive. Similarly, during the desorption stage, as the desorption time extended from 1 h to 4 h, the intensity of the DNA characteristic bands in the recovery solution significantly and progressively increased, and the electrochemical-applied group (−0.7 V, pH 10; lanes 6–9) had clearer and denser bands. The adsorption capacity and desorption efficiency of the electrochemical-applied group were significantly higher than those of the passive diffusion control. These results confirm that the applied electrochemical stimulation provides a strong driving force, significantly accelerating the migration speed of nucleic acid molecules.

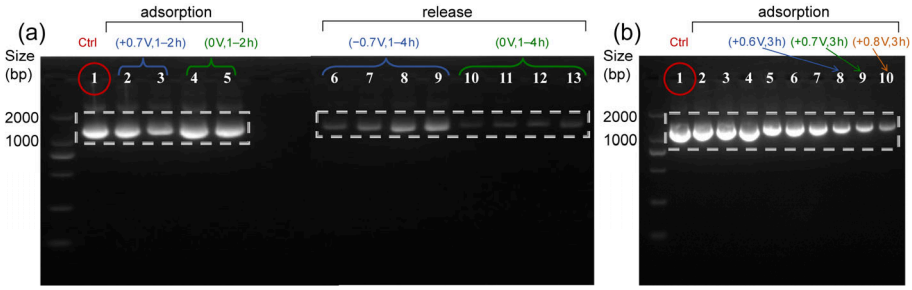


Figure 5. Electrochemical-driven DNA adsorption performance and voltage optimization. (**a**) The comparison of DNA adsorption/release efficiency between electrochemical-applied and passive diffusion modes (lane 1: raw DNA stock; lanes 2–3: electrochemical adsorption at pH 3.5 and +0.7 V; lanes 4–5: passive adsorption at pH 3.5 for 1 and 2 h; lanes 6–9: electrochemical release at pH 10.0 and −0.7 V; lanes 10–13: passive release at pH 10.0 for 1–4 h, respectively). (**b**) Optimization of adsorption voltage (+0.6, +0.7, and +0.8 V) at pH 3.5 (lane 1: untreated DNA; lanes 2, 5, and 8; lanes 3, 6, and 9; and lanes 4, 7, and 10: electrochemical adsorption at +0.6, +0.7, and +0.8 V for 1–3 h).

Next, the adsorption potential was optimized. Further evaluation was conducted at pH 3.5 for the adsorption effects under different applied positive voltages (+0.6 V, +0.7 V, +0.8 V) at different times (1–3 h) (Figure 5b). As time elapsed, the gray scale of the residual DNA bands in the supernatant rapidly decreased. At 3 h of adsorption, the DNA bands in the supernatant of the +0.7 V (lane 9) and +0.8 V (lane 10) potential groups were significantly lower than those of the +0.6 V (lane 8) potential group, demonstrating a faster adsorption rate. Although +0.8 V offers slightly faster adsorption, it approaches the critical value for PANI over-oxidation [39], which might threaten the long-term cyclability stability of the film and the safety of DNA. Consequently, +0.7 V is selected as the optimal adsorption potential to balance adsorption efficiency, electrode durability, and molecular integrity.

Finally, a synergistic optimization of the environmental pH value and reverse potential during the release stage was carried out. The comparison test of the release under different pH conditions (Figure 6a) indicates that the elution efficiency of DNA is highly dependent on the acidity and alkalinity of the environment. Under the same reverse voltage drive at −0.7 V, in a strongly alkaline environment (pH 10), a very dense and bright target band (lane 13) could be observed after 1 h of release, and almost all the DNA was recovered within 3 h (lane 19). This is because the strongly alkaline environment can more thoroughly deprotonate the amine/imine groups on the PANI molecular chains, eliminating the positive charge adsorption sites. Meanwhile, the reversed negative interface potential generates a stronger electrostatic repulsion on negatively charged DNA.

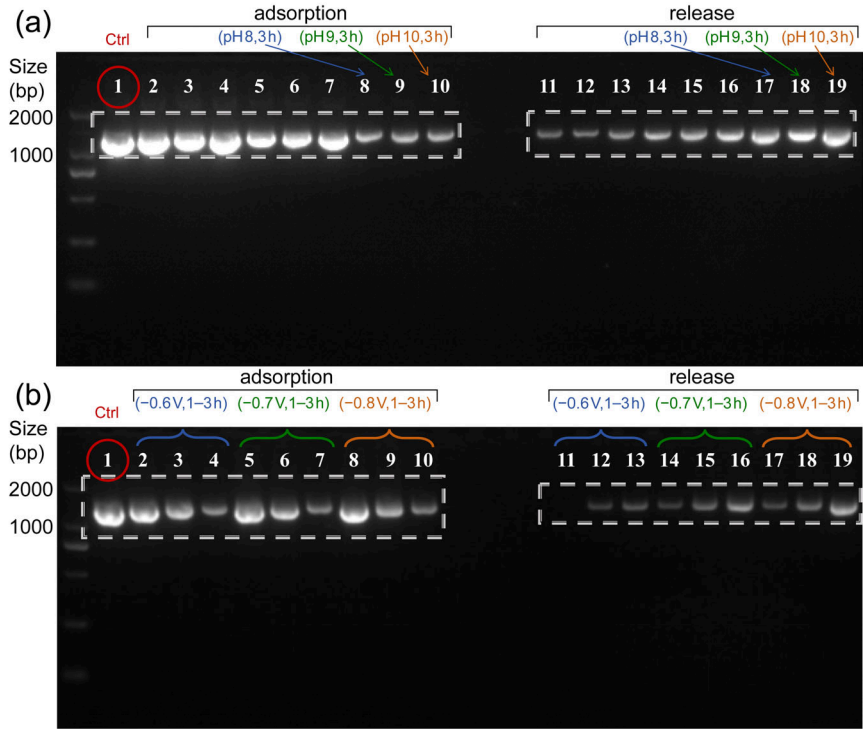


Figure 6. Optimization of desorption pH and reverse potential for DNA elution. (**a**) The effect of desorption pH value on DNA elution efficiency (lane 1: raw DNA; lanes 2–10 correspond to electrochemical adsorption for 1 h (lanes 2–4), 2 h (lanes 5–7), and 3 h (lanes 8–10) at pH 3.5, respectively; lanes 11, 14, and 17; lanes 12, 15, and 18; and lanes 13, 16, and 19: electrochemical-release at pH 8, 9, and 10 for 1–3 h). (**b**) The effect of reverse voltage on DNA elution efficiency (lane 1: untreated DNA; lanes 2–10: correspond to electrochemical adsorption for 1 h (lanes 2, 5, 8), 2 h (lanes 3, 6, 9), and 3 h (lanes 4, 7, 10); lanes 11–13, 14–16, and 17–19: correspond to electrochemical release at −0.6, −0.7, and −0.8 V for 1, 2, and 3 h, respectively).

Under the fixed optimal pH value of 10, the reverse voltage gradient test (Figure 6b) further demonstrated that when the absolute reverse potential increased from −0.6 V (lanes 11, 14, 17) to −0.7 V (lanes 12, 15, 18), the gray level of the DNA bands in the elution solution significantly enhanced, confirming that a higher negative potential can provide a stronger electrophoretic driving force for DNA release. Although the −0.8 V (lanes 13, 16, 19) potential group could exhibit a relatively higher elution band intensity, this potential may exceed the electrochemical stability window of PANI and might endanger the structural durability of the film and the integrity of the nucleic acid molecules [39]. In summary, this study established an optimal adsorption condition of "pH 3.5, +0.7 V" and a release condition of "pH 10.0, −0.7 V".

4. Conclusions

To address the bottlenecks of conventional solid-phase DNA storage media, such as the frequent nucleic acid cleavage caused by the use of chemical elution solutions and the reagent residue contamination, this study constructed a smart electrochemical-responsive PLA/PANI conductive composite film. The strategy of "brief alkaline modification followed by in-situ wet polymerization" was adopted to introduce hydrophilic functional groups on the surface of PLA fibers, thereby forming a dense and continuous PANI conductive network. This approach not only effectively maintains the structural integrity of the PLA scaffold, but also overcomes the limitations of conventional coatings such as easy blistering and drying-induced pore collapse, significantly enhancing the surface wettability, electrical conductivity, and thermal stability of the composite film. More importantly, the

film sensitively responds to the specific electrochemical and acid–base environments (pH 3.5, +0.7 V/pH 10.0, −0.7 V) to trigger the reversible transformation of the protonation state and electrostatic charge at the PANI interface, thereby achieving intelligent control of DNA adsorption/desorption. The PLA/PANI conductive composite film constructed in this study establishes a green and highly efficient solid-phase electrochemical-regulated DNA adsorption and release system, demonstrating broad application prospects in large-scale digital DNA data storage, specific addressing, and high-throughput random access.

Author Contributions: Conceptualization, H.L. and Z.M.; Methodology, Y.L. and Y.T.; Investigation, Y.L., Y.T. and L.L.; Data Curation, Y.L. and L.L.; Writing—Original Draft Preparation, Y.L.; Writing—Review & Editing, H.L.; Supervision, Z.L.; Project Administration, H.L. and Z.M.; Funding Acquisition, Z.L. All authors have read and agreed to the published version of the manuscript.

Funding: This work was supported by the National Key Research and Development Program (No. 2024YFF1206200).

Institutional Review Board Statement: Not applicable.

Informed Consent Statement: Not applicable.

Data Availability Statement: All data are available from the corresponding authors upon reasonable requests.

Conflicts of Interest: The authors declare no conflicts of interest.

References

1. Akash, A.; Bencurova, E.; Dandekar, T. How to Make DNA Data Storage More Applicable. *Trends Biotechnol.* **2024**, *42*, 17–30. [CrossRef]
2. Lim, D.; Kang, T.; Lee, W.; Haider, Z.; Noh, S.; Yu, M.; Huang, X.; Eun, H.S.; Song, Y. Electric Field–Guided Random-Access DNA Data Storage. *Sci. Adv.* **2026**, *12*, eadh1234. [CrossRef]
3. Dong, Y.; Sun, F.; Ping, Z.; Ouyang, Q.; Qian, L. DNA Storage: Research Landscape and Future Prospects. *Natl. Sci. Rev.* **2020**, *7*, 1092–1107. [CrossRef]
4. Liu, Q.J.; Liu, Q.; Zhang, J.; Zhang, C.; Qian, L.; Qi, H.; Li, Y.S.; Song, D.P. Photonic Microspheres for High-Capacity DNA Data Storage: Robust, Straightforward, and Scalable Random Access via Nonfading Indexes. *Sci. Adv.* **2025**, *11*, eado5678. [CrossRef]
5. Organick, L.; Ang, S.; Chen, Y.J.; Lopez, R.; Yekhanin, S.; Makarov, K.; Parker, J.; Strauss, K.; Ceze, L. Random Access in Large-Scale DNA Data Storage. *Nat. Biotechnol.* **2018**, *36*, 242–248, Erratum in *Nat. Biotechnol.* **2018**, *36*, 660. [CrossRef]
6. Liu, Q.; Wei, Y.; Wang, Z.; Song, D.; Cui, J.; Qi, H. Sustainable DNA Data Storage on Cellulose Paper. *Small Methods* **2023**, *7*, 2300123. [CrossRef]
7. Tan, X.; Ge, L.; Zhang, T.; Lu, Z. Preservation of DNA for Data Storage. *Russ. Chem. Rev.* **2021**, *90*, 280–291. [CrossRef]
8. Liu, B.; Wang, F.; Fan, C.; Li, Q. Data Readout Techniques for DNA-Based Information Storage. *Adv. Mater.* **2025**, *37*, 2400999. [CrossRef]
9. Gao, Y.; Ma, B.; Chen, G.; Xu, C.; Kong, Z.; Chen, Y.; Zhao, C.; Chen, D.; Yu, W.; Liu, H. Transformable and Stimuli-Responsive Liquid Metal for Integrated, Sustainable, and Biomimetic DNA-Based Data Storage. *Matter* **2025**, *8*, 102145. [CrossRef]
10. Wetzl, C.; Soukarie, D.; Yeregui Elosua, J.; Santiago, I. Integrating DNA-Based Memory in Water-Resistant Electrospun Polymer Fibers for Nondestructive Data Retrieval. *ACS Appl. Mater. Interfaces.* **2025**, *17*, 46089–46098. [CrossRef]
11. Zhao, Q.; Liang, X.; He, C. Efficient DNA Separation and Purification Via Vips-Constructed Membrane Adsorbers. *J. Membr. Sci.* **2024**, *690*, 122150.
12. Zhang, Y.L.; Shi, Y.J.; Duan, B.J.; Wang, X.H. One-Pot Hydrothermal Synthesis of Polyethyleneimine-Coated Magnetic Nanoparticles for High-Efficient DNA Extraction of Pathogenic Bacteria. *J. Chromatogr. B* **2025**, *1252*, 124435. [CrossRef]
13. Wang, C.; Wang, W.; Qi, H.; Dai, Y.; Jiang, S.; Ding, B.; Wang, X.; Li, C.; Zeng, J.; Wu, T.; et al. Electrospinning and Electrospun Nanofibers: From Academic Research to Industrial Production. *Prog. Mater. Sci.* **2025**, *154*, 101494. [CrossRef]
14. Mishra, R.K.; Mishra, P.; Verma, K.; Mondal, A.; Chaudhary, R.G.; Abolhasani, M.M.; Loganathan, S. Electrospinning Production of Nanofibrous Membranes. *Environ. Chem. Lett.* **2018**, *17*, 767–800. [CrossRef]
15. Zhang, J.H.; Zhang, J.; Zhang, X.; Wang, X.; Zhang, Z.; Sun, X.; Wang, H.; Liu, Z.; Sun, N.; Pan, L. Three-Dimensionally Microarchitected Electrospun Fabric-Enabled Pressure-Sensitive Bioelectronics. *MedMat* **2026**, *3*, 127–131. [CrossRef]

16. Bai, Y.; Meng, H.; Li, Z.; Wang, Z.L. Degradable Piezoelectric Biomaterials for Medical Applications. *MedMat* **2024**, *1*, 40–49. [CrossRef]
17. Haro Gutiérrez, P.A.; Colombi, S.; Casanovas, J.; Resina, L.; Sans, J.; Engel, E.; Enshaei, H.; García-Torres, J.; Pérez-Madrigal, M.M.; Alemán, C. Engineering Poly(Lactic Acid)-Based Scaffolds for Abundant, Sustained, and Prolonged Lactate Release. *ACS Polym. Au* **2025**, *5*, 247–260. [CrossRef]
18. Chen, Y.; Geever, L.M.; Killion, J.A.; Lyons, J.G.; Higginbotham, C.L.; Devine, D.M. Review of Multifarious Applications of Poly (Lactic Acid). *Polym.-Plast. Technol. Eng.* **2016**, *55*, 1057–1075. [CrossRef]
19. Li, G.; Zhao, M.; Xu, F.; Yang, B.; Li, X.; Meng, X.; Teng, L.; Sun, F.; Li, Y. Synthesis and Biological Application of Polylactic Acid. *Molecules* **2020**, *25*, 5023. [CrossRef]
20. Ilyas, R.N.; Zuhri, M.Y.M.; Aisyah, H.A.; Asyraf, M.R.M.; Hassan, S.A.; Zainudin, E.S.; Sapuan, S.M.; Sharma, S.; Bangar, S.P.; Jumaidin, R.; et al. Natural Fiber-Reinforced Polylactic Acid, Polylactic Acid Blends and Their Composites for Advanced Applications. *Polymers* **2022**, *14*, 202. [CrossRef]
21. Decorosi, F.; Exana, M.L.; Pini, F.; Adessi, A.; Messini, A.; Giovannetti, L.; Viti, C. The Degradative Capabilities of New Amycolatopsis Isolates on Polylactic Acid. *Microorganisms* **2019**, *7*, 5. [CrossRef]
22. Wang, Y.; Wang, R.; Zhao, Q.; Tian, Y.L.; Li, K.; Liu, L.Y.; Zhao, N.; Jiang, S.; Zhu, Y.; Li, N.; et al. Biomedical Applications of Polymer Porous Materials: Design, Properties, and Future Perspectives. *MedMat* **2025**, *3*, 132–146. [CrossRef]
23. Hao, Z.; Wang, Z.; Wang, Y.; Dong, M.; Zhang, Z.; Chen, J.; Shi, G.; Wang, J.; Chen, R.; Li, Z.; et al. Electrospinning for Mimicking Bioelectric Microenvironment in Tissue Regeneration. *Research* **2025**, *8*, 0959. [CrossRef]
24. Wang, T.; Shang, X.; Wang, H.; Wang, J.; Zhang, C. Experimental Investigation of Electrostatic Spinning of Polylactic Acid Porous Nanofibers. *J. Micromech. Microeng.* **2024**, *34*, 095007. [CrossRef]
25. Georgiev, V.; Ivanov, E.; Batakliev, T.; Kotsilkova, R. Composition-Dependent Thermoresistive Behavior of PLA/PCL/GNP Composites: From Monotonic PTC Response to Tunable PTC–NTC Transition. *Micro* **2026**, *6*, 34. [CrossRef]
26. You, J.; Liu, S.; Liang, J.; Feng, Q.; Duan, M.; Ali, Z.; Chen, L.; Wang, Z. Adaptive Dual-Responsive Nanocapsules for Precision Ferroptosis-Driven and Chemotherapy-Enhanced Tumor Ablation. *MedMat* **2024**, *1*, 104–117. [CrossRef]
27. Cabrera Gonzalez, A.D.; Flores León, J.R.; Ramirez Mendoza, C.G.; Rodríguez Félix, D.E.; Castillo Ortega, M.M.; Santacruz Ortega, H.; Rodríguez Félix, F.; Madera Santana, T.J.; Quiroz Castillo, J.M. Preparation and Characterization of Poly(Lactic Acid) Membranes and Films Coated with Polyaniline for Potential Use in Environmental Remediation. *ACS Omega* **2024**, *9*, 4439–4446. [CrossRef]
28. Jiang, B.; Wang, B.; Zhang, L.; Sun, Y.; Xiao, X.; Yang, N.; Dou, H. Improvement of Antifouling Performance of Poly(L-lactic Acid) Membranes through Incorporating Polyaniline Nanoparticles. *J. Appl. Polym. Sci.* **2017**, *134*, 44437. [CrossRef]
29. Fu, R.; Wang, C.; Zhuang, J.; Yang, W. Adsorption and Desorption of DNA on Bovine Serum Albumin Modified Gold Nanoparticles. *Colloids Surf. A Physicochem. Eng. Asp.* **2014**, *444*, 326–329. [CrossRef]
30. Li, Y.; Li, X.; Liu, Z.; Wang, Y.; Jiao, T. Recent Progress in the Strategies and Applications of Electrospinning Electroactive Tissue Engineering Scaffolds. *ACS Biomater. Sci. Eng.* **2025**, *11*, 3182–3200. [CrossRef]
31. Beygisangchin, M.; Abdul Rashid, S.; Shafie, S.; Sadrolhosseini, A.R.; Lim, H.N. Preparations, Properties, and Applications of Polyaniline and Polyaniline Thin Films—A Review. *Polymers* **2021**, *13*, 2003. [CrossRef]
32. Zhang, K.; Han, L.; Cai, H.; Xue, X.; Song, Y.; Xin, W.; Wang, Y.; Liu, P.; Liu, J. Toward Personalized Healthcare: Advances in Two-Dimensional Nanomaterial-Based Flexible Electrochemical Sensors for Physiological Monitoring. *BMEMat* **2025**, *4*, e12088. [CrossRef]
33. Kim, H.; Kim, H.Y.; Koo, J.H.; Cha, G.D.; Kim, D.; Kim, H.J. Fiber-Type Soft Bioelectronics for Wearable and Implantable Sensing and Therapy. *BMEMat* **2025**, *4*, e12095. [CrossRef]
34. He, X.; Li, Z.; Huang, X.; Zhang, Q.; Zeng, Y.; Li, J.; Yiu, C.K.; Yang, Y.; Zhou, J.; Xu, G.; et al. Sweat-Powered, Skin-Adhesive Multimodal Sensor for Long-Term and Real-Time Sweat Monitoring. *BMEMat* **2025**, *3*, e12124. [CrossRef]
35. Kharade, P.M.; Thombare, J.V.; Dhasade, S.S.; Deokar, S.S.; Salunkhe, D.J.; Tamboli, M.S.; Patil, S.S. Spongy-Network-like Polyaniline Thin Films as Electrodes for a Supercapacitor. *Micro* **2022**, *2*, 541–548. [CrossRef]
36. Ashraf, S.S.; Frounchi, M.; Dadbin, S. Gamma Irradiated Electro-Conductive Polylactic Acid/Polyaniline Nanofibers. *Synth. Met.* **2020**, *259*, 116204. [CrossRef]
37. Flores León, J.R.; Quiroz Castillo, J.M.; Rodríguez Félix, D.E.; Castillo Ortega, M.M.; Cabrera-González, A.D.; Ramirez-Mendoza, C.G.; Santacruz-Ortega, H.; Suárez-Campos, G.; Valenzuela-García, J.L.; Herrera-Franco, P.J. Preparation and Characterization of Extruded PLA Films Coated with Polyaniline or Polypyrrole by In Situ Chemical Polymerization. *ACS Omega* **2023**, *8*, 43243–43253. [CrossRef]

38. Huang, J.; Kaner, R.B. Nanofiber Formation in the Chemical Polymerization of Aniline: A Mechanistic Study. *Angew. Chem.* **2004**, *116*, 5941–5945. [CrossRef]
39. Stilwell, D.E.; Park, S. Electrochemistry of Conductive Polymers: II. Electrochemical Studies on Growth Properties of Polyaniline. *J. Electrochem. Soc.* **1988**, *135*, 2254–2262. [CrossRef]

Disclaimer/Publisher's Note: The statements, opinions and data contained in all publications are solely those of the individual author(s) and contributor(s) and not of MDPI and/or the editor(s). MDPI and/or the editor(s) disclaim responsibility for any injury to people or property resulting from any ideas, methods, instructions or products referred to in the content.